Available online at www.sciencedirect.com
ScienceDirect
Catalysis Today 129 (2007) 313–321
CATALYSIS TODAY
www.elsevier.com/locate/cattod

Hydrogen production from ethanol over bimetallic Rh-M/CeO_2 (M = Pd or Pt)

P.Y. Sheng, W.W. Chiu, A. Yee, S.J. Morrison, H. Idriss *

Department of Chemistry, The University of Auckland, Private Bag 92019, Auckland, New Zealand

Available online 29 September 2007

Abstract

The reaction of ethanol for the production of hydrogen has been studied over a series of metal supported CeO_2 catalysts. The study is conducted by TPD, steady state reaction, XPS, TEM, and infrared spectroscopy. TPD gave evidence for the role of Rh in dissociating the carbon–carbon bond needed for efficient production of hydrogen molecules. IR of CO adsorption at 90 K revealed that Rh particles are most likely in very small clusters as evidenced by a single O≡C–Rh IR band at 2020 cm^{-1}. TEM did not show conclusive evidence for the presence of the metal on-top of the CeO_2 support, yet the Rh-Pd/CeO_2 used catalyst has features that might be attributed to epitaxial growth of the noble metal along the (1 1 1) surface of the CeO_2 support. Considerable reconstruction of the CeO_2 support is seen for the used catalysts, in addition. Reforming of ethanol to hydrogen using (3 moles of water per mole of ethanol) was very efficient particularly above 650 K where hydrogen selectivity reaches 60 vol.%. At these temperatures hydrogen production from reforming of methane takes place.

Keywords: Ethanol reforming; Hydrogen production; Carbon–carbon bond dissociation; CO adsorption; Rh-Pd/CeO_2; Ethanol-TPD; XPS Ce3d; Pd3d; Rh3d

1. Introduction

Ethanol has been receiving considerable attention recently because of its high potential for producing molecular hydrogen to power fuel cells. At present the primary global energy demand is around 15 TW and bioenergy has the potential to contribute by up to 3 TW annually. Bioenergy in general suffers from its low energy density, about 1 W/m^2 (to compare to fossil fuel where the energy density is 10^3–10^4 W/m^2) [1]. Finding new processes or improving the present ones is thus highly desirable. Ethanol is attractive due to its renewable nature since it can be produced, in high yield by fermentation of crops, and thus has a negligible contribution into the overall CO_2 production. Because ethanol can be easily transported, on board hydrogen generation by reforming is an attractive solution to feed fuel cells. Catalytic reactions of ethanol both, as an end product, and as a reactant have been studied for long years with publications dating back to the early seventies [2–6]. Ethanol synthesis is particularly challenging since making one molecule of ethanol from two molecules of CO requires the dissociation of one molecule of CO. This reaction has been achieved over several noble metals supported catalysts including Rh [7–9]. Other ''non-C–O bond dissociating'' noble metals such as Pd could also be active with the addition of promoters such as alkali earth [10,11]. Within the principle of micro-reversibility it is thus not surprising that catalysts found appropriate for ethanol decomposition to hydrogen and carbon oxides are very similar to those found active for making it. For example, it has been observed almost 80 years ago that Cu/ZnO catalysts are equally good for making methanol from CO and H_2 as well as for decomposing the former to the latter compounds [12]. One main criterion in fully decomposing ethanol to H_2 and ''ideally'' to CO_2, is that the reaction intermediate should not include ethylene, the latter is formed by dehydration. Ethylene may further react to higher hydrocarbons and this does not only consume further hydrogen it may also lead to considerable deactivation of the catalyst due to un-desorbed high molecular weight compounds. In this case it has been seen that the support plays a crucial role. Acidic oxides such as Al_2O_3 are found to make considerable amounts of ethylene when used to support Rh. On the other hand basic oxides such as CeO_2 do not orient to the dehydration reaction [13,14]. CeO_2 has additional advantages that make it attractive: high oxygen storage capacity and being easily made

* Corresponding author. Fax: +64 9 373 7422.
E-mail address: h.idriss@auckland.ac.nz (H. Idriss).

0920-5861/$ – see front matter © 2007 Elsevier B.V. All rights reserved.
doi:10.1016/j.cattod.2006.09.040

of homogenous size particles of very small size; typically less than 20 nm in diameter.

To make Hydrogen from ethanol in a catalytic reaction several requirements need to be fulfilled [15]. First, the metal used need to be efficient in dissociating the C–C bond of ethanol. To do this one needs, ideally, to break one C–H of the terminal $–CH_3$ group. This has been reported to occur via an oxametallacycle intermediate. Rh and Co metals have been shown to stabilize this intermediate [16–18]. Second, the support needs to be active for water gas shift reaction to maximize the hydrogen yield [19] and this is most likely related to the capacity of the oxide to undergo oxidation/reduction cycles without deactivation. Third, the metal needs to be active for the H:H recombination reaction.

In this work we present a study of bimetallic Rh-containing CeO_2 catalyst and of its activity for ethanol reforming to hydrogen. The work is compared to other monometallic CeO_2 catalysts previously studied [20–27]. We have opted for Pd as a second metal because of its high hydrogenation activity and for Rh because of its activity for the C–C bond dissociation of ethanol molecule over CeO_2 [28].

2. Experimental

2.1. Catalyst preparation

CeO_2 was prepared by precipitating white crystalline cerous nitrate ($Ce(NO_3)_3{\cdot}6H_2O$) (100 g), dissolved in de-ionized water (0.40 L). Ammonia (0.91 mol L^{-1}) was added drop wise (ca. 30 mL) until a pH of 8 was attained. The resulting white slurry precipitate was than collected by filtration, washed and left to dry in an oven at 373 K for 12 h. The pale purple dried powder was calcined in a furnace at 773 K for 4 h with flowing air. Stock solutions of Pd and Rh metals, in 1 M of HCl were used. The monometallic and bimetallic catalysts $M–M'/CeO_2$ were prepared by conventional impregnating technique, where the CeO_2 support and the appropriate amount of stock solutions were mixed in a beaker at ambient temperature with continuous stirring. Temperature was than raised to around 373 K and retained. When most of the liquid vaporized, it forms paste like material, which was than dried for 12 h at 373 K then calcined for 4 h at 673 K under flowing air.

2.2. Characterization

Catalysts characterization was conducted by BET (QUANTASORB JR.), XRD (Philips 1130 generator and a Philips 1050 goniometer; Cu Kα: λ = 1.5148 Å), TEM (JOEL FX-2000II with a Link Isis EDX system), EDX and XPS (KRATOS XSAM-800, Al Kα X-ray (1486.6 eV); all peak energies were referenced to the C 1s binding energy of residual carbon at 284.7 eV) techniques. Table 1 presents some of the characterization results. In brief the main characteristics of the catalysts were as follow.

1. The BET surface area of CeO_2 alone or that after metal impregnation deviated mildly. This was mainly due to reproducibility of the precipitation method rather than to an intrinsic effect of the metal ions (because of the very low concentration of the metal). The BET values ranged from 50 to 80 m^2/g.
2. CeO_2 alone did not contain Ce^{3+} ions but all other ‘‘as prepared’’ catalysts did contain non-negligible amounts of Ce^{3+} (Fig. 1).
3. The atomic percentage of the elements on the surface differed from the expected bulk composition, most likely due to surface segregation (Fig. 1).
4. The fluorite bulk structure was maintained for all catalysts.
5. TEM did not conclusively identify the presence of the metals on the surface of CeO_2, which had an average diameter close to 20 nm. Yet both XPS and EDX did detect their photoelectron (XPS) and X-ray (EDX) emission.
6. Irreversible (titration at 300 K) and electrostatic (90 K) adsorption of CO gave evidence of considerable differences in the CO mode of adsorption between CeO_2 and M/CeO_2.

The last two points (5 and 6) will be treated in more details in Section 3.

2.3. Catalytic reactions

2.3.1. Temperature programmed desorption

Ethanol reactions were performed in a conventional U-shape quartz fixed bed micro-reactor. Samples (∼50 mg) were loaded onto the sinter of the reactor. Prior to any reactions, sample

Table 1
Measured surface atomic percentage by XPS from the integrated (and corrected) XPS Ce 3d, Rh 3d, Pd 3d, Pt 4f and O 1s lines for different catalysts

Catalyst (BET surface area m^2/g catalyst)	Surface at.% M/CeO_2 (XPS)	M/CeO_2 based on bulk composition (at.%)	XPS O 1s/Ce 3d	CO uptake at 300 K (molecule m^{-2})
Rh/CeO_2 (49)	0.17 (0.21)[a]	1.68	1.91	39×10^{16}
Pd/CeO_2 (55)	0.25 (0.28)[a]	1.61	1.76	5×10^{16}
Pt/CeO_2 (63)	0.26 (0.31)[a]	0.90	1.59	9×10^{16}
$Rh-Pd/CeO_2$ (84)	0.86 (0.85)[a,b]	1.68–1.61	1.56	11×10^{16}
$Rh-Pt/CeO_2$ (36)	0.42 (0.44)[a,b]	1.68–0.90	1.66	57×10^{16}

Also shown the expected percentage based on bulk composition. The binding energy of the metal indicates that they are mainly in an oxidized state, as indicted, although signal contribution from metallic states cannot be ruled out. The CO uptake at 300 K is conducted, over hydrogen-reduced samples at 523 K for 12 h, 1 atm, by the pulse method (0.25 ml injection volume of CO). No detectable CO uptake was found for CeO_2 alone at the indicated conditions. The O 1s/Ce 3d ratios are an indication of the extent of reduction of the support by the metal at the calcination conditions (673 K).

[a] Numbers in parentheses are reported excluding surface carbon contamination

[b] Atomic percentage of Rh and Pd are 0.46 and 0.40, respectively, while those of Rh and Pt are 0.21 and 0.21, respectively.

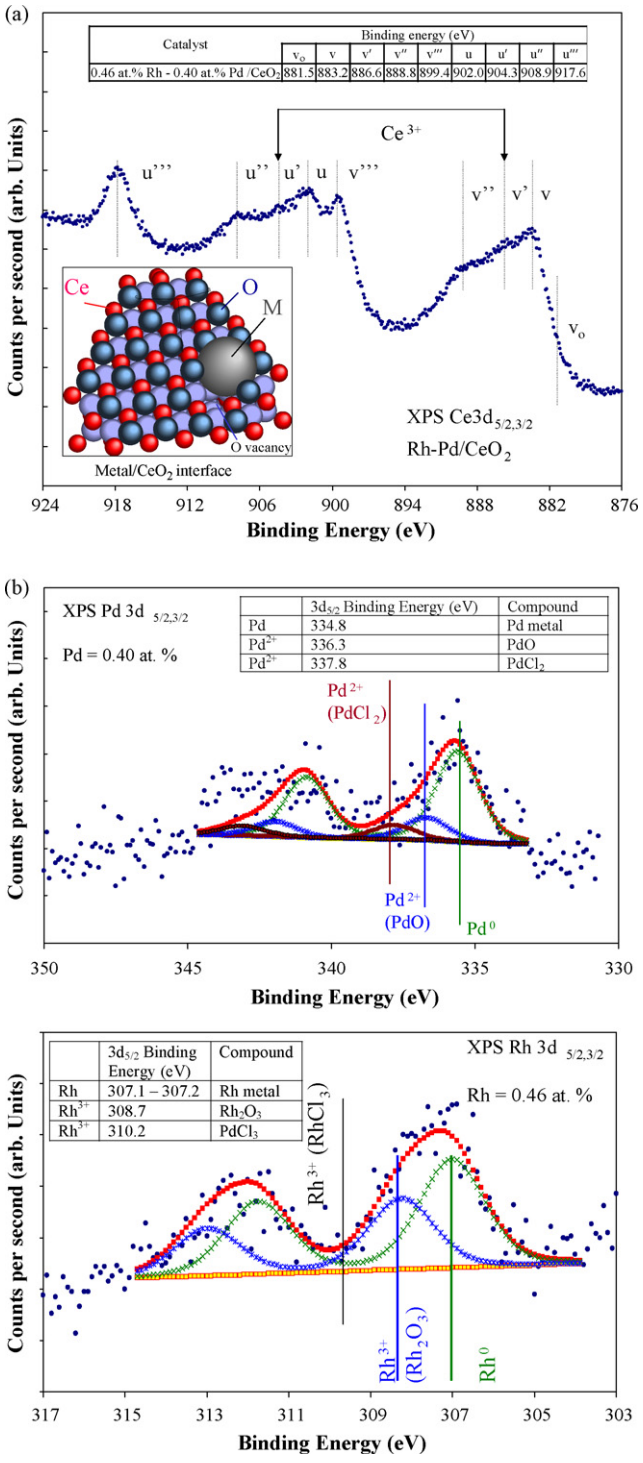

Fig. 1. (a) Typical XPS Ce 3d-lines of a metal impregnated over CeO_2 support. The presence of Ce^{3+} lines is indicative of metal induced surface reduction of a part of CeO_2. The Ce^{3+} lines are not observed on a similarly treated CeO_2 without the noble metal (Metals used were Rh, Pd or Pt with the atomic percentage indicated in Table 1). (b) XPS 3d levels for the Pd and Rh contributions of the 0.46 at.% Rh–0.40 at.% Pd/CeO_2. While the presence of the metal is clear a non-negligible contribution of the metal oxide is also seen. $RhCl_3$ is clearly not present while small Pd 3d lines that can be attributed to $PdCl_2$ cannot be excluded. Binding Energies of Rh and Pd lines are from Ref. [53].

catalysts were oxidized at 573 K under oxygen stream for 3 h. The reactor was than allowed to cool to ambient temperature under oxygen, then pumped down to base pressure ($\sim 10^{-2}$ Torr). Dosing of ethanol was done by allowing its vapor pressure (about 8 Torr at room temperature) to saturate the catalyst bed for a period of 3 min, sufficient for complete monolayer coverage. After dosing, the reaction line was then subject to further pumping to remove any loosely adhered reactant on the catalyst surface and in the line. The reactor was than heated using a high temperature-heating furnace connected to a programmed temperature controller. The reaction line was connected to the vacuum chamber containing a Spectra Vision quadrupole mass spectrometer, with a base pressure of 10^{-7} Torr. Before data collection, the signal at $m/z = 31$ (dominant fragment of ethanol) was monitored. The TPD (from 300 to 773 K with ramping rate of 20 K min^{-1}) started when no further change was observed. The desorption profile was monitored inside the high vacuum chamber using the quadrupole mass spectrometer, connected to an online computer and running a mass spectrometer software (RGA for Windows), which allows the monitoring of up to 200 masses simultaneously at a cycle rate of 1 min or up to 12 masses at a faster cycle rate (typical 5 s/cycle). Relative yields were calculated for individual desorption products by quantitatively analyzing the desorption spectra for the respective mass fragments. In order to identify a gas from mass spectra, the fragmentation pattern of a particular species must be known. Two factors were employed when determining the cracking contribution; firstly, major fragmentation product was distinguished from the background signal, and secondly, assigning possible products to the fewer possible species. In the case of a mass fragment resulting from multiple species other mass fragments were checked for consistency. The method used for TPD analysis is the same as that reported in other works [21–23].

2.4. Infrared spectroscopy

Infrared spectra were monitored using a Digilab FTS-60 Fourier transform spectrometer, with a 256 scan data acquisition at a resolution of 4 cm^{-1}. The adsorption of ethanol on sample catalysts were performed in a stainless steel IR cell equipped with removable CaF_2 windows (32 mm diameter, 4 mm thick) sealed with Viton O-rings. The calcium fluoride optics is used to monitor the region from 4500 to 1000 cm^{-1} regime and is capable of operating at temperatures between 77 and 773 K. A type K (chromel/alumel) thermocouple, welded into the center of the cell in close proximity to the catalyst disc, was used to monitor the temperature. The sample catalysts was pressed into a self-supporting disc (ca. 15 mm in diameter), and mounted into a gold-plated brass sample holder inside the cell. The cell is connected to a vacuum line, with a base pressure of ca. 10^{-5} Torr. O_2 and CO gases used to treat the catalyst were contained in separate glass bulbs, which were attached to the vacuum line by vacuum-sealed clamps. Catalysts were annealed under 20 Torr of O_2 at 673 K followed by evacuation for 1-h. The cell was then cooled to the desired temperature prior to adsorption.

3. Results and discussion

Fig. 1a presents a typical XPS Ce3d of an "as prepared" Rh-Pd/CeO_2 catalyst. The XP spectra of ceria are rather complicated due to the hybridization between the Ce 4f levels and the O 2p state. The series of peaks denoted by v and u are from the $3d_{5/2}$ and $3d_{3/2}$ states of Ce, respectively. Both Ce $3d_{5/2}$ and Ce $3d_{3/2}$ levels are composed of five components, three structures in the case of CeO_2 and two structures only for Ce_2O_3. They are identified as (v_0, v, v′, v″ and v‴) and (u_0, u, u′, u″ and u‴), if the spin-orbit coupling is taken into account. Assignment of the different structure shown is with referring to the work from Burroughs et al. [29], as represented by several other workers [30–36], where structures of v, v″ and v‴ are attributed to CeO_2. The hybridization between the Ce 4f screening level and the O 2p level results in the v and v″ lines, which are due to a mixture of $Ce(5d\ 6s)^0\ 4f^2\ O2p^4$ and $Ce(5d\ 6s)^0\ 4f^1\ O2p^5$ configurations, respectively.[106] The v‴ line is a pure $Ce(5d\ 6s)^0\ 4f^0\ O2p^6$ final state. On the other hand, v_0 and v′ are due to mixture of $Ce(5d\ 6s)^0\ 4f^2\ O2p^5$ and $Ce(5d\ 6s)^0\ 4f^1\ O2p^6$ final states in Ce_2O_3. The u structures of Ce $3d_{3/2}$ level can be explained in a similar way. Owing to the complexity of the spectra, no quantitative analysis was attempted as to the partitioning of the Ce^{4+} and Ce^{3+} species. It is however clear that Ce^{3+} ions are present because of the lines assigned to v′ and u′. The nine transitions observed in this work (the 10th transition, u_o, is generally not observed in a CeO_2/Ce_2O_3 mixture because it is masked by the v″ peak) are shown in the inset of Fig. 1a. Fig. 1b presents the XPS 3d lines corresponding to Rh and Pd. The atomic percent for both metal is relatively low and explains the high signal to noise. It is however clear that a combination of metal and metal oxides is present for both metals. The Pd region was more difficult to analyze. The raw data could not be fitted with two peaks at each line ($3d_{5/2}$ and $3d_{3/2}$). Because some chlorine atoms are left on the surface upon calcination, it is possible to attribute the third peak in each region not to another oxidation state of Pd but to ligands-effect (chlorine has a higher electronegativity value than oxygen and as a results the core electron of Pd^{2+} in $PdCl_2$ appears with a higher binding energy when compared to Pd^{2+} in PdO).

The extent of reduction has been related to the amount and nature of the noble metal that triggers the reduction of a fraction of Ce^{4+} ions on the surface [15]. The inset in Fig. 1a is a schematic representation of the (1 1 1) CeO_2 phase (the most stable surface in a fluorite structure) in presence of a metal. The reduction of Ce^{4+} ions is most likely occurring at the interface with the metal and is presented in the inset by a missing O atom. Table 1 gives the atomic percent of surface atoms (as analyzed by XPS) together with the expected atomic percentage of the metals if they were equally distributed in the bulk and at the surface. All metal/CeO_2 catalysts contained an O to Ce ratios less than 2, indicating some reduction of the surface of ceria. Also shown is the CO uptake at 300 K over the catalysts. CO adsorption was not observed on CeO_2 alone in this work suggesting that irreversible adsorption at 300 K on the support is negligible compared to that on the metal. No attempt was made to calculate the metal particle size because of inevitable variations in the modes of adsorption of CO on the different metals.

Infrared spectra of sequential irreversible CO adsorption on CeO_2 and Rh/CeO_2 at 90 K and after evacuation under dynamic vacuum (10^{-4} Torr) are presented in Fig. 2A and B. Both catalysts were not reduced prior to CO adsorption. The objective is to see for a possible differences in the weak (electrostatic) mode of adsorbed CO on Ce and on Rh cations. The introduction of small amounts of CO (0.4 Torr), Fig. 2A, leads to the appearance of a band in the CO stretching region at 2186 cm^{-1}. A gradual increasing of the CO pressure results in

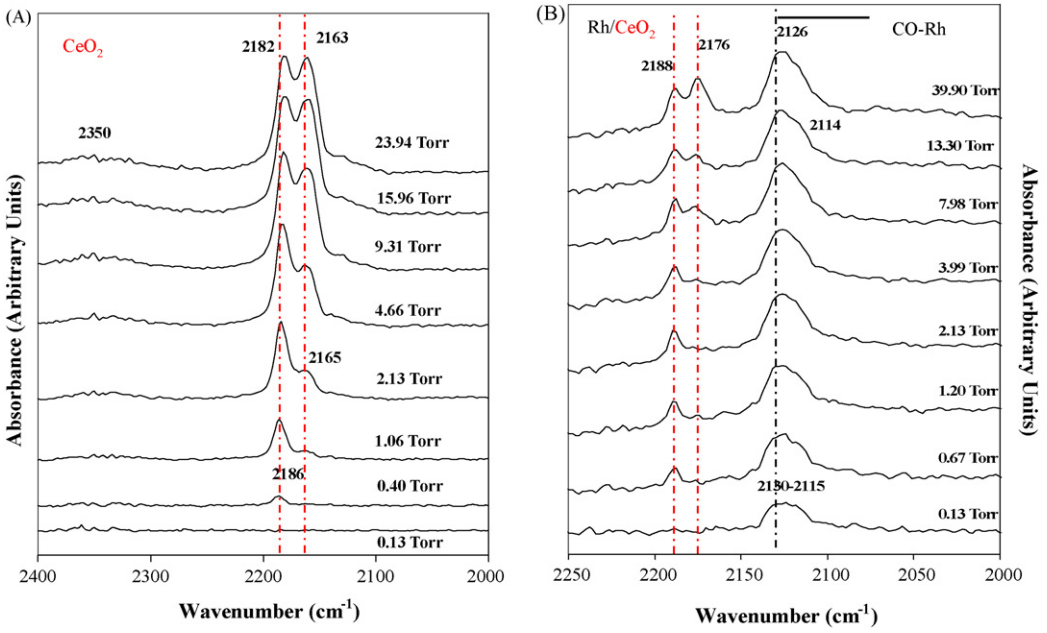

Fig. 2. FT-IR of irreversible CO adsorption over (A) CeO_2 and (B) Rh/CeO_2 at 90 K with increasing CO pressures. Data collection was performed at ≈10^{-4} Torr. Note the presence of CO at ca. 2120 cm^{-1} in the presence of Rh.

an intensity increase of the 2186 cm^{-1} band and an emergence of a lower wavenumber shoulder at about 2165 cm^{-1}. Further increase of the CO pressure enhanced the intensity of both bands. The shoulder at 2165 cm^{-1} eventually shared similar absorbance intensity as the band at 2186 cm^{-1} at high coverage. At saturation coverage, the absorption bands at 2186 and 2165 cm^{-1} experienced negligible shifts to 2182 and 2163 cm^{-1}, respectively. In general a large shift with increasing coverage is associated with a large distribution of non-homogenous-type surfaces [37,38]. The assignment of these two bands is, however, not totally clear at present. Two C–O stretching bands of 2170 and 2150 cm^{-1} [39] or 2168 and 2157 cm^{-1} are observed by others [40] when adsorbing CO on CeO_2 at low temperature followed by evacuation. These two bands were assigned to CO adsorbed on Ce^{4+} cations and defects associated with Ce^{3+}, respectively. This interpretation is tempting; yet, the absence of Ce^{3+} by XPS in our CeO_2 ''alone'' may not favor such an argument. Although a small amounts of Ce^{3+} may escape the instrument resolution of about 0.5 eV, it is difficult to accept that ''stoichiometric'' CeO_2 has equal amounts of Ce^{4+} and Ce^{3+} at its surface. There are however other interpretations, one of them is based on different binding modes on differently oriented surfaces. An ab initio DFT study has attempted to compute the frequency of CO on CeO_2 as a function of surface structure [41]; CeO_2(1 1 1) and CeO_2(1 1 0). The authors [42] found that CO adsorbed on the (1 1 1) surface was blue shifted (from the CO gas phase) by +6 cm^{-1} while that on the (1 1 0) was shifted by +15 cm^{-1}. The blue shift is consistent with experimental observations of this work and those of others [37–40]. Although the absolute numbers do not match the experimental ones (in general due to deviation of the computation work from un-harmonicity), their result nevertheless points to another interpretation not related to different oxidation states of Ce ions. In their work they also found that the binding energy of CO is higher on the (1 1 0) when compared to that on (1 1 1) surface [41]. This is in line with the results of Fig. 2A since the high frequency band populates first. Heating to 180 K resulted in the removal of all CO from the surface (not shown). The presence of Rh ions (Fig. 2B) is clearly marked by the appearance of a band at about 2120 cm^{-1}. This band is attributed to a linear mode of adsorption (red shifted with respect to gas phase CO) on isolated (very small) clusters of Rh ions on point defect of CeO_2 for the reasons outlined next. IR bands of CO adsorbed on Rh have been well studied in the past. In particular and relevant to this work is the IR of CO at low temperature on Rh supported on oxide supports [42,43]. This IR and STM study of CO adsorption at 90 K (the same temperature as in this work) over clusters of Rh atoms (about 9 atoms) deposited over thin film of Al_2O_3 have shown that these small clusters give IR bands at 2117 cm^{-1} and at 2125 cm^{-1} attributed to linear CO–Rh ions [42,43] as well as to $(CO)_2$–Rh^+ species (gem dicarbonyl).

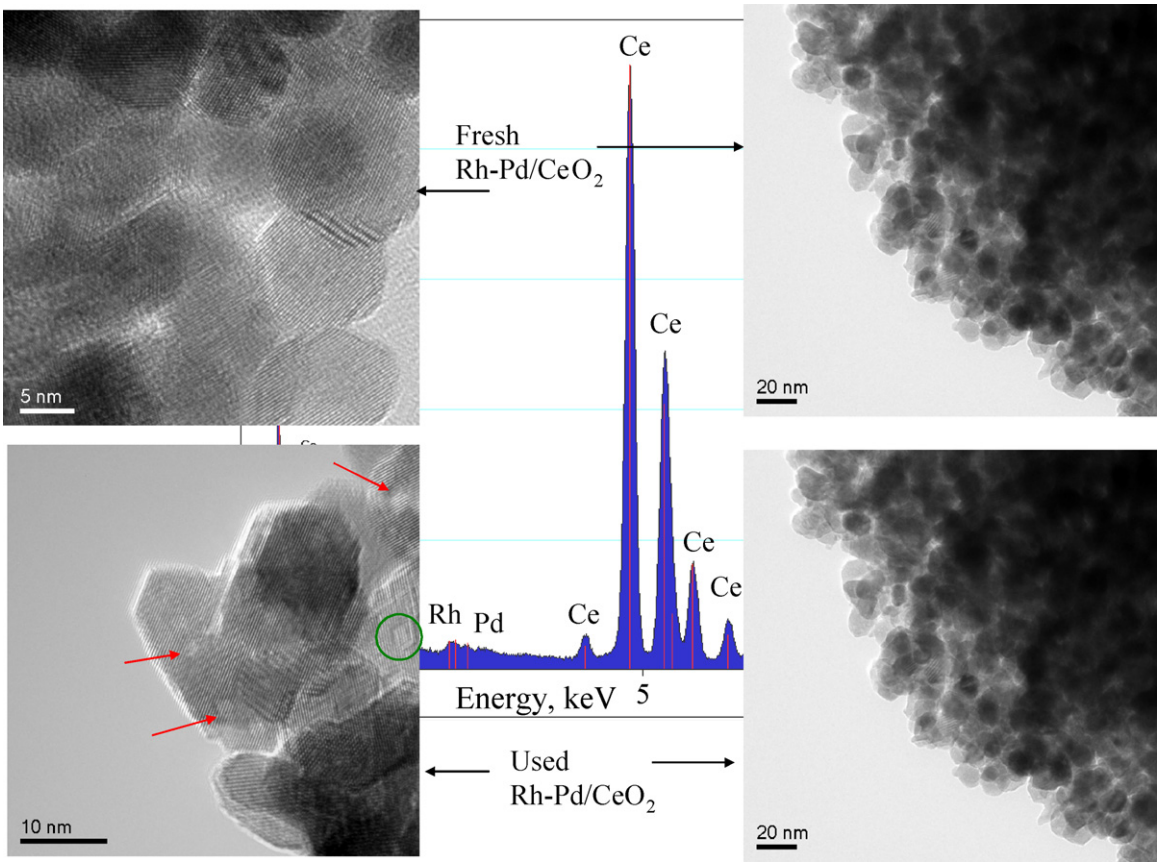

Fig. 3. TEM pictures of fresh and used Rh-Pd/CeO_2. CeO_2 particle size is about 20 nm in both cases. The used catalyst shows light features that can be attributed to reconstruction. The hexagonal shape structures may also indicate the presence of metal on top of the CeO_2. EDX graph (center) shows the presence of Rh and Pd in addition to Ce.

Based on STM data they have attributed this mode to Rh clusters formed on point defects (Figs. 1 and 2 of Ref. [32]). When the cluster size increases this band disappears in favor of a more commonly observed band around 2080 cm^{-1}. The authors explain the absence of the asymmetric band of the gem dicarbonyl (expected at about 2050 cm^{-1}) as possibly due to selection rule because of the thin film in their case [39,40]. This explanation is difficult to apply in our case because CeO_2 is polycrystalline. Thus the absence of a band at 2050 cm^{-1} in Fig. 2 may not be in favor of a dicarbonyl species and most of CO adsorbed on these isolated Rh ions is in the form of CO–Rh^{x+}. In addition, in our case (Fig. 2) the band is large and is most likely composed of more than one type of linearly adsorbed CO–Rh^{x+}. It is worth indicating that a computation work a decade ago has predicted that segregation of metal ions such as Pd^{2+}, and Rh^{3+} are stabilized with O point defects on the surface of CeO_2 [44]. In all cases the IR data favors the formation of Rh particles in small clusters. Following the initial population of these sites the two IR bands corresponding to adsorbed CO over Ce cations are seen as in the case of CeO_2 alone. Removal of O≡C-Rh bands occurs by heating the surface to 240 K (not shown).

Fig. 3 shows a TEM/EDX study of a fresh and used Rh-Pd/CeO_2 catalyst. Other M/CeO_2 catalysts were also studied and the results were in general similar. As in other works CeO_2 is composed of very small particles. High magnification reveals that the unused CeO_2 has lattice fringes mostly along the [1 1 1] orientation as expected from the most stable cut of the fluorite structure. Nothing else was observed on the fresh catalyst despite numerous attempts. In other words while EDX (inset of Fig. 3), XPS (Table 1), irreversible CO adsorption (Table 1) at room temperature and electrostatic CO-adsorption (Fig. 2B) show evidences of the presence of the metal the TEM pictures did not conclusively show that. The used catalyst (for the reforming of ethanol with a total number of working hours of about 60) had other features, however. Two distinct regions in some particles (denoted as 1 and 2) are seen in Fig. 4. First, light patches of hexagonal shape are present (region 1). The line spacing is close to 3.7 ± 0.2 Å, within the instrument resolution, which is very close to that of the spacing along the (1 1 1) plan of CeO_2 (3.8 Å). The spacing of Pd (1 1 1) or Rh (1 1 1) is far smaller 2.8 Å. In other words if these lines belong to Pd or Rh (or a mixture of both) they would have grown epitaxially on top of a CeO_2 lattice. Second, light feature with lozenge shapes are also seen (region 2). One can also see steps along the edges. Reconstructions giving rise to steps, is not uncommon. The first fluorite-type surface to give rise to steps is the (3 1 0). This surface has been postulated as the most active low index surface for CO oxidation [45] it does also have he highest surface energy of low index surfaces of CeO_2 [46]. It is not intended to explain the reconstruction of CeO_2 as solely due to the formation of the 310 reconstructed-phase alone, though. The inset in Fig. 4 shows a schematic representation of such a stepped surface (as an example).

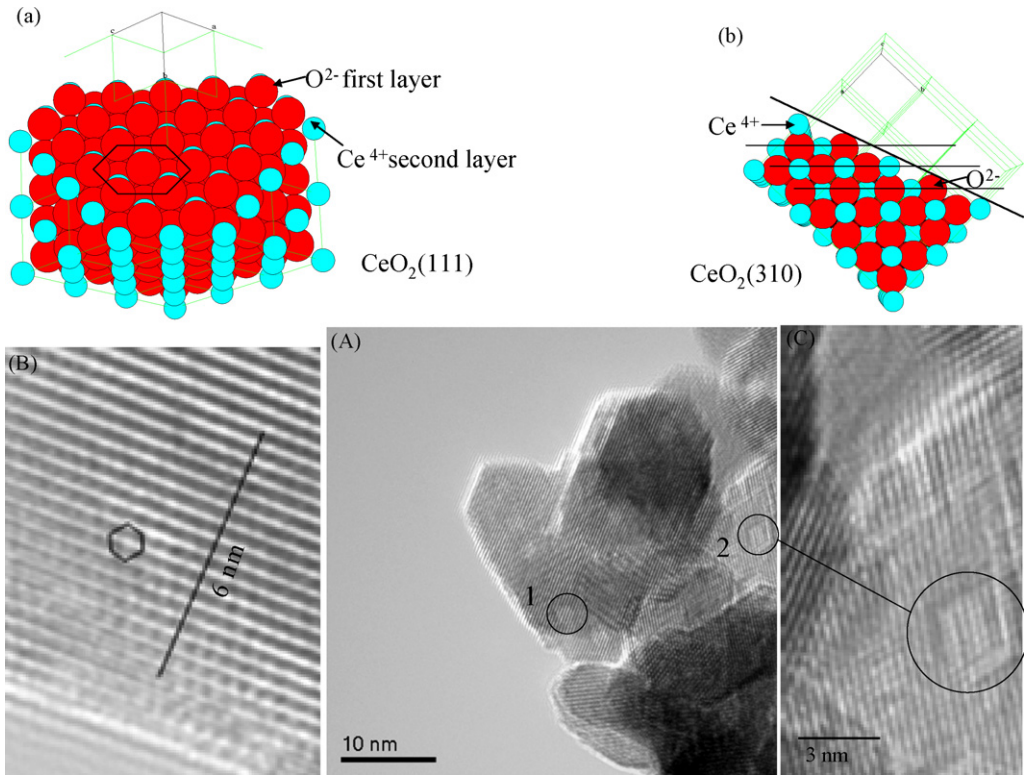

Fig. 4. (A) TEM of a used Pd-Rh/CeO_2 catalyst (the same region as the middle one of Fig. 3). Highlighted are two regions denoted by 1 and 2. (B) A typical TEM micrograph of a CeO_2 surface, note that the line spacing and lattice configuration are consistent with a hexagonal packing arrangement of 3.7–3.8 Å as expected for the (1 1 1) phase of the fluorite structure of CeO_2. (C) Region 2 in (A) is magnified presenting step-type reconstructions. The inset is a representation of two surfaces of the fluorite CeO_2 structure. (a) The most stable (1 1 1) surface where the compact hexagonal structure is seen. (b) A stepped structure the (3 1 0) as an example, where the ions have a lower coordination numbers at the step edge, the solid line is along the (3 1 0) plane.

Table 2
Selectivity of reaction products during Ethanol-TPD over Rh-Pd, Rh-Pt and Pd-Pt bimetallic catalsyts

Reaction product[a]	Rh-Pd/CeO_2		Rh-Pt/CeO_2		Pt-Pd/CeO_2	
	Unreduced	Reduced	Unreduced	Reduced	Unreduced	Reduced
Acetaldehyde	23.6 (410)	3.2 (435)	26.2 (460)	7.1 (460)	30.1 (435)	36.5 (445)
Methane	3.8 (410)	44.2 (495, 665)	7.4 (475)	38.7 (460, 670)	5.7 (435)	6.0 (445, 665)
CO	22.2 (575)	14.4 (665)	29.7 (620)	18.1 (18.1)	23.3 (600)	29.5 (665)
CO_2	50.4 (575)	38.0 (665)	36.7 (620)	35.9 (670)	40.9 (600)	27.8 (665)

The numbers in parentheses indicate TPD peak desorption temperature, T_{max}. Unreduced catalysts were heated in O_2 at 773 K while reduced catalysts were heated in H_2 at 523 K, prior to TPD experiments, other details can be found in Section 2.
[a] The reaction products in percentage excluding un-reacted ethanol.

From Figs. 1–4 one can conclude that (i) part of CeO_2 is reduced by the presence of the noble metal ions (Pd, Rh, or Pt), (ii) the presence of these noble metal ions is also seen following CO adsorption at 90 K by IR. (iii) these metals (as well as metal ions) are not unambiguously seen by TEM; this at least indicates that their particle dimension is smaller than ≈5 nm, (iv) reconstruction of part of CeO_2 surface occurs for the used Rh-Pd/CeO_2 catalyst.

Ethanol TPD was conducted on several monometallic and bimetallic catalysts, containing Rh, Pt and Pd on CeO_2 and details of some are given in Refs. [21–23,25,26,28]. Although Ethanol-TPD is conducted in conditions not necessarily close to those of reforming or oxidation reactions it brings essential information needed for the study of ethanol reaction. Here we focus on three TPD studies over the bimetallic catalysts: Rh-Pd/CeO_2, Rh-Pt/CeO_2 and Pd-Pt/CeO_2. Table 2 shows details of the desorption products quantified as indicated in Section 2. The reaction product distribution on the bimetallic catalysts is very simple, in contrast to that observed over the monometallic catalysts [21–23]. This is indicative of the high activity of the bimetallic catalysts for ethanol decomposition. This high activity is of course due to the higher loading of the support (see Table 1) but is essentially due to a combined (synergetic) effect of the Rh with Pd or Pt as explained next. Other products that were observed on the monometallic catalysts but are not observed here are acetone and benzene. Water in all cases was not quantified and ethylene in all cases was absent. There is one main observation from Table 2: catalysts containing Rh give a large amount of methane when they are hydrogen reduced prior to TPD. Hydrogen reduction will reduce metal ions to zero valent metal. The behavior is best explained in Fig. 5. While the three unreduced catalysts behave similarly for ethanol decomposition and give considerable amounts of acetaldehyde the reduced catalysts containing Rh switch the reaction from acetaldehyde to methane. On the contrary the reduced Pd-Pt/CeO_2 does not show much difference. In other words the carbon–carbon bond splitting of ethanol is not further improved by reduction of Pd or Pt ions. Oxidative dehydrogenation of ethanol yields acetaldehyde and this is naturally more favored over unreduced catalysts. Reduction may still favor dehydrogenation if beta hydrogen elimination of the ethoxide species (formed upon dissociative adsorption of ethanol as seen by IR on these catalysts [21–23,28 among others] occurs. However, Rh metal favors the removal of terminal hydrogen of the CH_3 group and this results in an oxametallacycle intermediate:

$$CH_3CH_2O(a) \rightarrow CH_3CHO(g) + H(a)$$

favored over Pd and Pt metals

$$CH_3CH_2O(a) \rightarrow (a)\text{-}CH_2\text{-}CH_2O(a)$$ favored over Rh metal

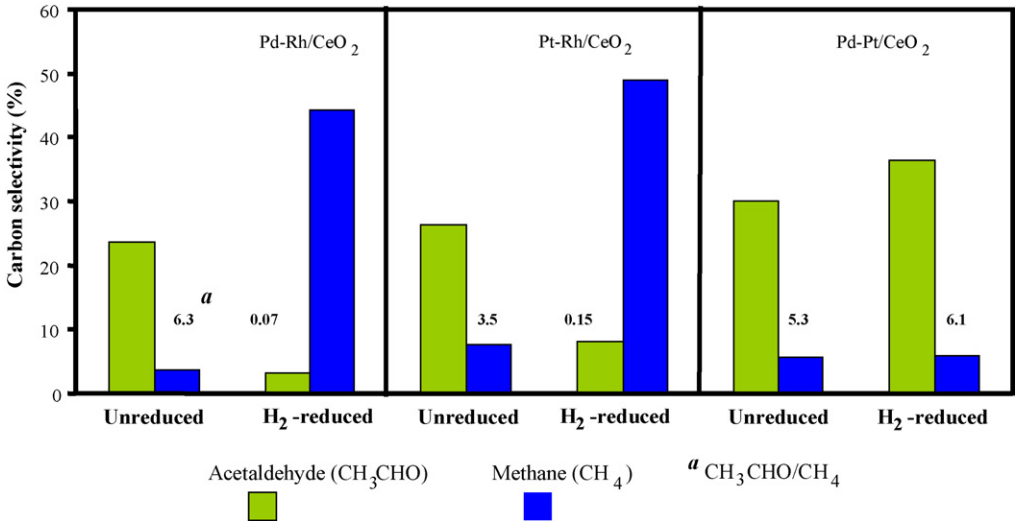

Fig. 5. Acetaldehyde and methane carbon selectivity during ethanol-TPD of three bimetallic catalysts. The numbers indicate acetaldehyde to methane ratio for the unreduced and H_2-reduced catalysts.

Periodic Pane wave DFT study of Rh/CeO_2 (1 1 1) surface indicated that the decomposition of ethanol has a low energy path via an oxametallacycle intermediate at the interface between Rh and Ce ions: $Rh–CH_2CH_2O–Ce$ [47]. This route is in line with the above experimental observation.

Fig. 6 presents the reforming of ethanol with water (1 ethanol/3 water molecules) over $Rh\text{-}Pd/CeO_2$ as a function of temperature. The catalyst was not reduced prior to reaction. At each temperature the catalyst was kept for a period of 2 h or more. No catalytic deactivation is seen during this period. The numbers indicated are the average over about a 2-h period. At low temperature <500 K trace amounts of acetaldehyde and acetone are seen. These products were absent at higher temperatures. Ethylene was not observed at all temperatures studied consistent with TPD results. Ethanol has almost totally reacted at temperatures >650 K. There are two main observations in the figure. (i) The 550–650 K temperature-interval is very critical for CO and CO_2 production. This observation has been repeated several times and is independent of reaction flow rate. Water gas shift reaction (WGSR) is most likely the reason. (ii) Above 700 K hydrogen production increases in detriment of methane, this is consistent with reforming of methane and has been seen on other studies [48–50]. However, the amount of CO increases again at high temperature. It is worth indicating that WGSR is exothermic while reforming is endothermic [more details on the temperature effects on these two reactions can be found in Ref. [51]]. The steam reforming reaction (SRR) together with WGSR have been studied over a wide range of catalysts in order to find the best catalytic formulation for hydrogen and CO_2 production [52]. It was found that while Rh is very good for SRR the presence of a good WGSR such as CeO_2 has resulted in a decrease of the CO_2 formation at high temperature. The authors therefore have concluded that a non-active support for the WGSR should be used. The authors presumably indicate that CO_2 can be directly formed by CO oxidation in a different route. This interesting idea may need complementary work for further understanding.

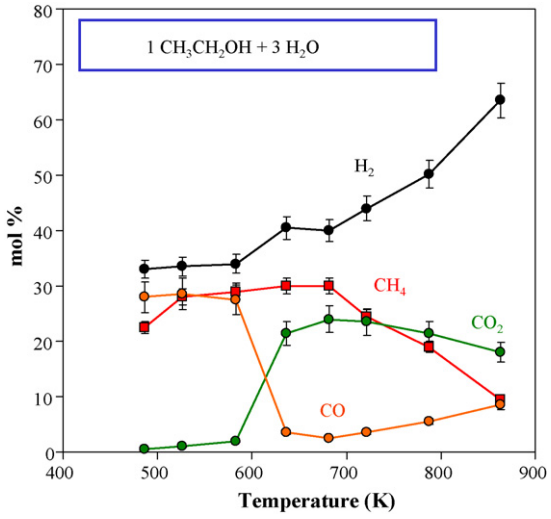

Fig. 6. Product distribution during ethanol reforming with water (molar ratio = 3 water to 1 ethanol molecule) over $Rh\text{-}Pd/CeO_2$ catalyst as a function of reaction temperature. P = 1 atm, F(liquid)/W = 5 L/kg h

The complete reaction was repeated four times (the duration of each run was about 15 h). The trend was reproducible indicating that the catalyst was not deactivated. Maximum variations of the reaction yield of 10–15% were observed. These variations are attributed to analytical and experimental errors rather than to an intrinsic change within the catalyst from one run to the other.

4. Conclusions

The reaction of ethanol has been studied over bimetallic CeO_2 catalysts (Rh and Pd or Pt) for the production of hydrogen. The reaction seems to occur at the interface between Ce and metal ions. While CO adsorption (IR and titration), XPS and TPD techniques revealed characteristics related to the presence of the metal, TEM does not give conclusive presence. It is highly likely that these metals are dispersed in ultra small clusters on the surface of the support. The presence of Rh atoms is crucial for the reforming of ethanol since they initiate the terminal carbon–hydrogen bond dissociation and thus favoring the formation of the possible oxametallacycle intermediate needed for further interaction with the surface and dissociation of the carbon–carbon bond. The increasing hydrogen production at elevated temperatures (above 650 K) is most likely due to reforming of methane. The formation of methane is undesired and the next generation of catalysts will need to suppress methane formation if a low temperature (below 650 K) hydrogen production catalyst by reforming of ethanol is desired.

Acknowledgments

The authors would like to acknowledge Peter Buchanan (University of Auckland) for his technical support and Mark Blackford (Australian Nuclear Science and Technology Organization) for collecting the TEM data. Part of this work was conducted by a research grant number AINGRA05077P from the Australian Institute for Nuclear Science and Engineering and by a University of Auckland VC award.

References

[1] R. Doornbosch, S. Upton, Do we have the right R&D priorities and programmes to support the energy technologies of the future, OECD SG/SD/RT, 2006, p. 1, http://www.oecd.org/dataoecd/47/9/37047380.pdf.
[2] M.M. Bhasin, G.L. O'Cornor, Belgian Patent 824,822 (1975).
[3] M.M. Bhasin, W.J. Bartley, P.C. Ellgen, T.P. Wilson, J. Catal. 54 (1978) 120.
[4] M. Ichikawa, Bull. Chem. Soc. Jpn. 51 (1978) 2273.
[5] M. Ichikawa, J. Chem. Soc. Chem. Commun. (1978) 566.
[6] A. Sugier, E. Freund, U.S. Patent, 4,122,110 (1978).
[7] A.S. Lisitsyn, S.A. Stevenson, H. Knözinger, J. Mol. Catal. 63 (1990) 201.
[8] H. Ehwald, H. Ewald, D. Gutschick, M. Hermann, H. Miessner, G. Öhlmann, E. Schierhorn, Appl. Catal. 76 (1991) 153.
[9] A. Kiennemann, R. Breault, J.P. Hindermann, M. Laurin, J. Chem. Soc. Farad. Trans. I 83 (1987) 2119.
[10] C. Diagne, H. Idriss, J.P. Hindermann, A. Kiennemann, Appl. Catal. 51 (1989) 165.

[11] D. He, Y. Ding, H. Yin, T. Wang, H. Luo, C. Li, Catal. Lett. 84 (2002) 89.
[12] P.K. Frölich, M.R. Frenske, P.S. Taylor, C.A. Southwich Jr., Ind. Eng. Chem. 20 (1928) 1327.
[13] H. Idriss, E.G. Seebauer, J. Mol. Catal. A 152 (2000) 201.
[14] H. Idriss, E.G. Seebauer, Catal. Lett. 66 (2000) 139.
[15] H. Idriss, Platinum Met. Rev. 48 (2004) 105.
[16] N.F. Brown, M.A. Barteau, Langmuir 11 (1995) 1184.
[17] M. Mavrikakis, D. Doren, M.A. Barteau, J. Phys. Chem. 102 (1998) 394.
[18] G.S. Jones, M. Mavrikakis, M.A. Barteau, J.M. Vohs, J. Am. Chem. Soc. 120 (1998) 3196.
[19] R.J. Gorte, S. Zhao, Catal. Today 104 (2005) 18.
[20] H. Idriss, C. Diagne, J.P. Hindermann, A. Kiennemann, M.A. Barteau, Stud. Surf. Sci. Catal. 75 (1993) 2119.
[21] A. Yee, S. Morrison, H. Idriss, J. Catal. 186 (1999) 279.
[22] A. Yee, S.J. Morrison, H. Idriss, J. Catal. 191 (2000) 30.
[23] P.-Y. Sheng, A. Yee, G.A. Bowmaker, H. Idriss, J. Catal. 208 (2002) 393.
[24] C. Diagne, H. Idriss, A. Kiennemann, Catal. Commun. 3 (2002) 565.
[25] P.-Y. Sheng, G.A. Bowmaker, H. Idriss, Appl. Catal. A 261 (2004) 171.
[26] P.Y. Sheng, H. Idriss, J. Vac. Sci. Technol. A 22 (2004) 1652.
[27] C. Diagne, H. Idriss, K. Pearson, M.A. Gómez-García, A. Kiennemann, Comptes Rendus Chimie 7 (2004) 617.
[28] A. Yee, S.J. Morrison, H. Idriss, Catal. Today 63 (2000) 327.
[29] P. Burroughs, A. Hammett, A.F. Orchard, G. Thornton, J. Chem. Soc., Dalton Trans. (1976) 1686.
[30] H. Idriss, C. Diagne, J.P. Hindermann, A. Kiennemann, M.A. Barteau, J. Catal. 155 (1995) 219.
[31] F. Le Normand, J. El Fallah, L. Hilaire, P. Legare, A. Kotani, J.C. Parlebas, Solid State Commun. 71 (1989) 885.
[32] M. Romeo, K. Bak, J. El Fallah, F. Le Normand, L. Hilaire, Surf. Interface Anal. 20 (1993) 508.
[33] B. Ernst, L. Hilaire, A. Kiennemann, Catal. Today 50 (1999) 413.
[34] J. Rynkowski, J. Farbotko, R. Touroude, L. Hilaire, Appl. Catal. A: Gen. 203 (2000) 335.
[35] D.R. Mullins, S.H. Overbury, D.R. Huntley, Surf. Sci. 409 (1998) 307.
[36] A.Q. Wang, P. Punchaipetch, R.M. Wallace, J. Vac. Sci. Technol. B 21 (2003) 1169.
[37] E. Platero, S. Coluccia, A. Zecchina, Surf. Sci. 171 (1986) 465.
[38] D. Scarano, A. Zecchina, Spectrochim. Acta 43[a] (1987) 1441.
[39] M.I. Zaki, B. Vielhaber, H. Knozinger, J. Phys. Chem. 90 (1986) 3176.
[40] C. Binet, M. Daturi, J.C. Lavalley, Catal. Today 50 (1999) 207.
[41] Z. Yang, T.K. Woo, K. Hermansson, Chem. Phys. Lett. 396 (2004) 384.
[42] M. Frank, R. Kühnemuth, M. Bäumer, H.-J. Freund, Surf. Sci. 454–456 (2000) 968.
[43] M. Frank, R. Kuhnemuth, M. Baumer, H.J. Freund, Surf. Sci. 427 (1999) 288.
[44] T.X.T. Sayle, S.C. Parker, C.R.A. Catlow, J. Phys. Chem. 98 (1994) 13625.
[45] T.X.T. Sayle, S.C. Parker, C.R.A. Catlow, Surf. Sci. 316 (1994) 329.
[46] Y. Jiang, J.B. Adams, M. van Schilfgaarde, J. Chem. Phys. 123 (2005) 064701-1.
[47] H.-L. Chen, S.-H. Liu, J.-J. Ho, J. Phys. Chem. B 110 (2006) 14816.
[48] S. Cavallaro, V. Chiodo, S. Freni, N. Mondello, F. Frusteri, Appl. Catal. A: Gen. 249 (2003) 119.
[49] S. Cavallaro, V. Chiodo, A. Vita, S. Freni, J. Power Source 123 (2003) 10.
[50] A.N. Fatsikostas, X.E. Verykios, J. Catal. 225 (2004) 439.
[51] M.V. Twigg (Ed.), Catalyst Handbook, second ed., Wolfe, Frome, England, 1989.
[52] F. Auprêtre, C. Descorme, D. Duprez, Catal. Commun. 3 (2002) 263.
[53] D. Briggs, M.P. Seah, second ed., Practical Surface Analysis, vol. 1, Wiley, Chichester, England, 1996.